京都大学防災研究所年報　第46号　B　平成15年
Annuals of Disas. Prev. Res. Inst., Kyoto Univ., No. 46 B, 2003

Assessment of Undrained Seismic Displacements on Shear Surfaces in Saturated Cohesionless Soils

Aurelian C. TRANDAFIR, Kyoji SASSA and Hiroshi FUKUOKA

Synopsis

The present study is concerned with the seismic performance of an infinite slope in udrained conditions. The material on the sliding surface is assumed to be a saturated clean sand with the undrained shear strength characteristics provided by a laboratory study based on ring shear tests. The experimental outcomes from undrained monotonic and cyclic ring shear tests come to support a modified Newmark sliding block model for assessing the earthquake–induced undrained slope displacements. The proposed methodology incorporates in the computational process the ability of a saturated sand to withstand strain in dynamic conditions by using the experimental data from undrained monotonic shearing. Sample calculations concerning the undrained seismic slope response under different input seismic records, revealed that the seismic waveform affects the amount of earthquake–induced undrained permanent slope displacement. The softening of the material on the sliding surface has significant influence on the mobility of the sliding mass ensuing an earthquake–induced catastrophic slope failure.

Keywords: earthquakes; slopes; clean sand; ring shear tests; undrained shear strength; seismic stability

1. Introduction

Analysis of seismic performance of an infinite slope by Newmark's sliding block method (Newmark, 1965) represents a common engineering practice. The conventional Newmark procedure has been used extensively to develop empirical relationships between the expected permanent displacement of a sliding soil mass and related earthquake characteristics (e.g., Newmark, 1965; Sarma, 1973; Franklin and Chang, 1977; Maksidi and Seed, 1978; Ambraseys and Menu, 1988; Cai and Bathrust, 1995). Typically, these displacements functions have been obtained by making the crucial assumption that the yield resistance to sliding remains constant and equal to that mobilized at a factor of safety of one. Hence, the influence of variations in excess pore water pressure and rapid loading–unloading effects on the available shear resistance of the soil on the sliding surface, in relation to the seismically induced incremental displacements was not taken into account.

Goodman and Seed (1966) verified experimentally the Newmark's classical procedure by investigating the relationship between accelerations and displacements in a bank of cohesionless material subjected to ground displacements. One of the main outcomes of this study was that the computed values of displacements showed high sensitivity to minor changes in soil strength parameters. Consequently, a correct analysis of seismic displacements involves accurate knowledge of the shear strength that can be developed by the soil on the slip surface at a certain instant during the seismic excitation. In this framework, the present study addresses a modified Newmark formulation to estimate the earthquake–induced undrained displacements of a soil mass along a planar sliding surface consisting of a saturated cohesionless material.

During recent years, results of undrained monotonic and cyclic ring shear tests on saturated cohesionless soils have been reported in literature by Sassa and colleagues (Sassa, 1996; Sassa et al., 1997a; Wang, 1998; Wang et al., 2000; Sassa, 2002; Wang and Sassa, 2002). These experimental studies revealed that saturated sandy soils exhibiting a dilative shear behavior before failure, may be triggered to liquefy after reaching the failure

condition as the excess pore water pressure gradually continues to generate with increasing unidirectional shear displacement. This phenomenon was referred as "sliding surface liquefaction" (Sassa, 1996). Sliding surface liquefaction may result in ultimate steady state strengths smaller than the static driving shear stress making, therefore, the slope susceptible to a catastrophic failure under seismic conditions.

The goal of this research was to develop a procedure for assessing the undrained seismic displacements of an infinite slope along a slip surface composed of a saturated clean sand, susceptible to sliding surface liquefaction. To achieve this, a methodology representing a combination of conventional sliding block method (Newmark, 1965) and experimental data is proposed. The procedure makes use of the shear resistance–displacement curve obtained from undrained monotonic ring shear tests to approximate the available shear strength on the slip surface during earthquake. The accuracy of this assumption is verified by a laboratory study based on ring shear tests carried out on the considered sand. The experimental program consisted of undrained monotonic and cyclic ring shear tests on replicate samples, for a given initial stress state, aiming to compare the shear resistance–displacement relationship from monotonic loading with the available shear strength under various cyclic loading conditions (e.g., amplitude, frequency, waveform). The effectiveness of the proposed methodology is enhanced by sample calculations, concerning the undrained seismic performance of two infinite slopes subjected to real input earthquake accelerations.

2. Experimental Program

The undrained tests were carried out using an intelligent ring shear apparatus (DPRI-Ver.6) developed and improved upon by Sassa and colleagues (Sassa, 1997). A schematic layout along with a very detailed description of this equipment, emphasizing the undrained testing capabilities and the water-pressure measurement system, is presented elsewhere (Sassa, 1997; Sassa, 2000; Sassa et al. 2002*a*; Wang and Sassa 2002). The samples tested in DPRI-Ver.6 are about 135 mm in height, with an outer diameter of 350 mm and an inner diameter of 250 mm, respectively.

2.1 Sample characteristics

The present study is concerned with ring shear tests on silica sand no. 6 (S6), which mainly consists of quartz (92%-98%) and a small amount of feldspar. Examination of S6 under an optical microscope revealed that the grains are subrounded to subangular, as shown in Fig. 1. Table 1 summarizes the results of a series of laboratory tests performed to determine the gradation, specific gravity and the maximum/minimum void ratio of S6. The grain size distribution of S6 is also illustrated in Fig. 2. It is seen in Fig. 2 that S6 is uniform, with grain sizes ranging from 0.1 to 0.9 mm, and it has a negligible fraction of fines.

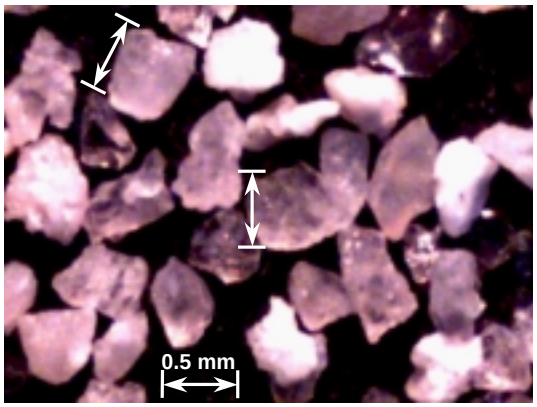

Fig. 1 Microscopic view of silica sand no. 6 (60x)

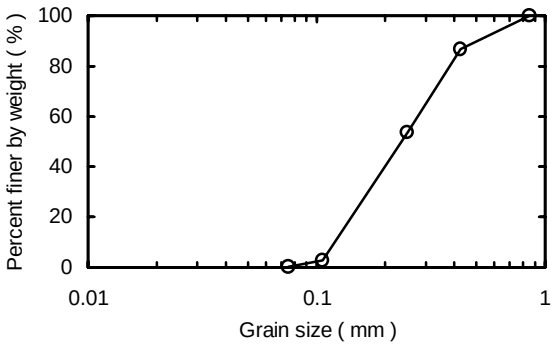

Fig. 2 Grain-size distribution of silica sand no. 6

Table 1 Properties of silica sand no. 6

Mean grain size, D_{50} (mm)	0.25
Effective grain size, D_{10} (mm)	0.115
Uniformity coefficient, U_c	2.4
Maximum void ratio, e_{max}	1.16
Minimum void ratio, e_{min}	0.69
Specific gravity, G_s	2.66

2.2 Sample preparation and testing procedure

The specimens were prepared by dry deposition method, that is the oven dried sample fell into the shear box freely through a plastic bottle like a funnel, from the top of the upper ring. The saturation was accomplished by aid of carbon dioxide and de-aired water after the sample has been poured in the shear box. The saturation degree was checked by calculating B_D parameter proposed by Sassa (1988) and given by Eq. (1):

$$B_D = \frac{\Delta u}{\Delta \sigma} \quad (1)$$

in which Δu stands for the increment of pore water pressure increase due to a change in total normal stress, usually from 50 to 100 kPa, i.e., $\Delta\sigma = 50$ kPa under undrained conditions. The specimen is assumed to be fully saturated when $B_D \geq 0.95$. All ring shear tests in this study satisfied the condition $B_D \geq 0.95$.

The experimental program included series of tests on normally consolidated specimens under effective normal stress levels of 150 and 250 kPa. After consolidation under an effective normal stress σ'_0, the shear stress was increased with a loading rate of about 0.5 kPa/sec in drained conditions to an initial value τ_0, in order to achieve the desired initial shear stress ratio, τ_0 / σ'_0. Undrained loading was subsequently applied in a monotonic or cyclic manner. Concerning the shear stress control system of DPRI-Ver.6, three rotating gears are available, capable to develop a maximum shear speed of 10 mm/sec, 32.3 cm/sec, and 2.24 m/sec, respectively. The medium rotating gear, corresponding to a maximum shear speed of 32.3 cm/sec, was employed for this experimental study.

2.3 Undrained monotonic shear behavior of saturated sand

After setting-up the initial shear stress, the shear box was shifted to undrained conditions and the sample was sheared by gradually increasing the shear stress with a loading rate of about 0.5 kPa/sec while maintaining constant the total normal stress. The gradual reduction in shear strength with progress of shear displacement, after failure, resulted in an accelerated motion until the shear velocity reached the limit value of 32.3 cm/sec.

Figure 3 shows the response of S6 to undrained monotonic shearing for two initial stress points (A and B in Fig. 3a), corresponding to initial effective normal stress levels of 150 and 250 kPa, and initial shear stress ratios of 0.25 and 0.5, respectively. In Fig. 3*b*, e_c denotes the void ratio immediately after consolidation (i.e., zero initial shear stress). Apparently, the sand demonstrated a quasi steady state (*QSS*) type of response (Ishihara, 1993) during yielding prior to failure. Figure 3*a* displays how after the first peak of shear resistance was reached, the stress path moves quickly towards the failure line due to significant generation of excess pore water pressure with straining. As pointed out by Yoshimine et al. (1999), the quasi steady state coincides with the state of phase transformation, subsequent shearing resulting in dilation associated with increase in shear strength towards a secondary peak, reached at the moment of failure.

After failure, the sand exhibited sliding surface liquefaction (Sassa, 1996), as shown by the effective stress path moving down along the failure line in Fig. 3*a*. The orders of magnitude of shear displacement, required to reach the ultimate steady state strength (*USS*) are noticeable in Fig. 3*b*.

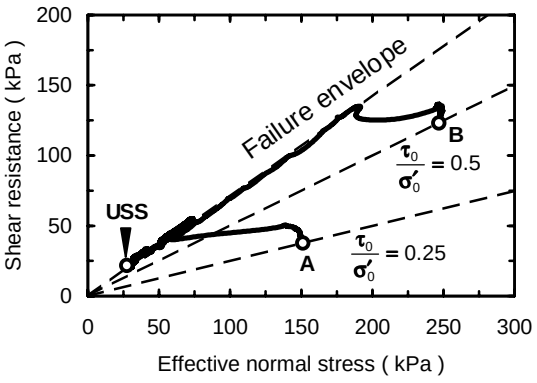

(a)

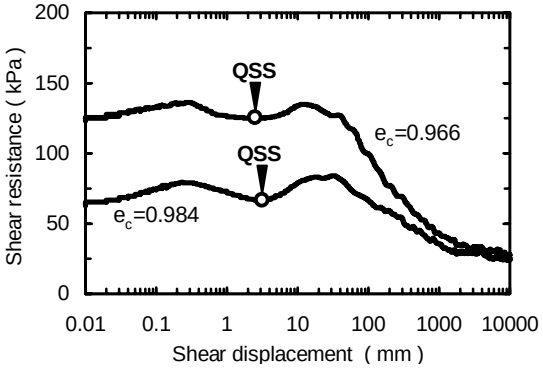

(b)

Legend:
USS – Ultimate Steady State, **QSS** – Quasi Steady State

Fig. 3 Effective stress paths (*a*) and shear resistance–displacement relationships (*b*) from undrained monotonic ring shear tests

2.4 Undrained cyclic ring shear tests

The primary objective of this laboratory study was to compare the shear resistance–displacement data obtained under undrained monotonic loading conditions, with the corresponding response of saturated sand to cyclic loading, for a given initial stress state. Consequently, undrained cyclic ring shear tests were carried out on replicate samples subjected to initial stresses defined, in the effective stress space, by points A and B from Fig. 3*a*. The experiments followed the same procedure described for the undrained monotonic ring shear tests except that, after setting up the initial stress state, the undrained loading was applied in a cyclic manner instead of monotonically.

The cyclic stresses for laboratory testing were selected in order to reproduce the dynamic conditions on the sliding surface of an infinite slope, subjected to a horizontal seismic excitation, as shown in Fig. 4.

The slope, with an inclination β, is assumed to have a phreatic surface located in–between the ground surface and the potential failure plane, and an average unit weight of the soil within the sliding mass, γ=18 kN/m^3.

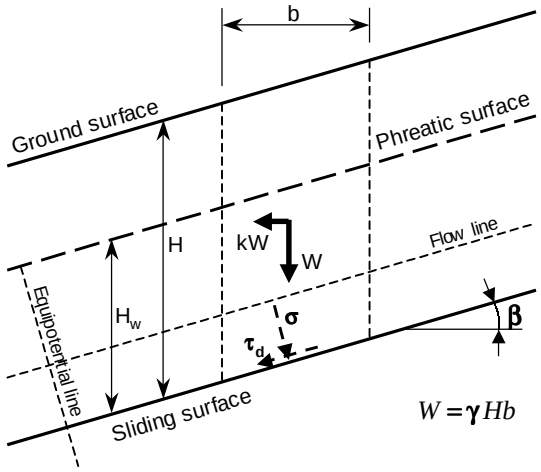

Fig. 4 Configuration of an infinite slope under seismic conditions

The expressions of initial total normal stress, σ_0, and driving shear stress, τ_0, on the sliding surface (i.e., static conditions) derived from the normal and tangential components of the weight, *W*, of a soil column of width *b*, in respect to the direction of slip surface, are as follows:

$$\sigma_0 = \frac{W\cos\beta}{b\sec\beta} = \gamma H\cos^2\beta \tag{2}$$

$$\tau_0 = \frac{W\sin\beta}{b\sec\beta} = \gamma H\sin\beta\cos\beta \tag{3}$$

where *H* stands for the height of the soil mass above the sliding surface.
From Eqs. (2) and (3) we obtain

$$\sigma_0 = \frac{\sigma'_0}{\tan\beta}\left(\frac{\tau_0}{\sigma'_0}\right) \tag{4}$$

For this study we consider a seepage parallel to the surface and a groundwater level at height H_w above the sliding plane, i.e., equipotential lines perpendicular onto the surface. In these circumstances, the initial pore water pressure, u_0, on the sliding plane may be expressed as

$$u_0 = \gamma_w H_w\cos^2\beta \tag{5}$$

where γ_w is the unit weight of water, taken in this study as 10 kN/m^3.

On the other hand, based on the effective stress principle u_0 can also be derived as

$$u_0 = \sigma_0 - \sigma'_0 = \frac{\sigma'_0}{\tan\beta}\left[\left(\frac{\tau_0}{\sigma'_0}\right) - \tan\beta\right] \tag{6}$$

Equations (2) to (6) enable us to express *H* and H_w as functions of σ'_0, τ_0/σ'_0, and β as follows:

$$H = \frac{2\sigma'_0}{\gamma\sin 2\beta}\left(\frac{\tau_0}{\sigma'_0}\right) \tag{7}$$

$$H_w = \frac{2\sigma'_0}{\gamma_w\sin 2\beta}\left[\left(\frac{\tau_0}{\sigma'_0}\right) - \tan\beta\right] \tag{8}$$

Concerning the applied seismic waveform, a sinusoidal excitation was assumed, with the general expression for the coefficient of earthquake acceleration, *k*, at a certain instant, *t*, given by

$$k = (k_0 + j\Delta k)\sin\left(2\pi\frac{t}{T}\right) \tag{9}$$

where *T* is the period of seismic excitation, and *j* = 1…*N* is the number of current cycle. *N* refers to the total number of cycles during the experiment. Two types of cyclic loading are engaged in this study, as illustrated in Fig. 5. The first type (Fig. 5*a*) corresponds to a gradual increase in the amplitude of earthquake acceleration by a constant increment, Δk, at the beginning of each cycle. This is equivalent with making $k_0 = 0$ in Eq. (9). The second type (Fig. 5*b*) considers a seismic excitation of constant amplitude, k_0, which actually corresponds to $\Delta k = 0$ in Eq. (9). The cyclic total normal stress, $\Delta\sigma$, and cyclic driving shear stress, $\Delta\tau_d$, on the sliding plane due to a horizontal inertia force imparted by the earthquake loading on the slope shown in Fig. 4, may be expressed as

$$\Delta\sigma = k\,\sigma'_0\left(\frac{\tau_0}{\sigma'_0}\right) \tag{10}$$

$$\Delta\tau_d = k\frac{\sigma'_0}{\tan\beta}\left(\frac{\tau_0}{\sigma'_0}\right) \tag{11}$$

Table 2 summarizes the initial stress conditions and cyclic loading characteristics for the undrained cyclic ring shear tests, along with the parameters of simulated infinite slope conditions.

In the time history of applied cyclic loading, the total normal stress, σ, and driving shear stress, τ_d,

Table 2 Summary of cyclic ring shear tests and equivalent infinite slope parameters

Initial stresses and test no.	e_c	Cyclic loading characteristics				Equivalent slope parameters		
		k_0	Δk	f (Hz)	N	β (°)	H (m)	H_w (m)
Case **A**: $\sigma'_0 = 150$ kPa ; $\tau_0 / \sigma'_0 = 0.25$								
A1	0.978	0.170	0	0.4	42	10	12.2	6.5
A2	0.981	0.350	0	0.4	20			
Case **B**: $\sigma'_0 = 250$ kPa ; $\tau_0 / \sigma'_0 = 0.5$								
B1	0.971	0	0.006	0.4	20	20	21.6	10.6
B2	0.967	0.125	0	0.2	10			

Note: f denotes the frequency of applied cyclic loading ($f = 1/T$)

acting on the sample at a certain instant during the experiment are given by the equations below:

$$\sigma = \sigma_0^* - \Delta\sigma \tag{12}$$

$$\tau_d = \tau_0 + \Delta\tau_d \tag{13}$$

with $\Delta\sigma$ and $\Delta\tau_d$ defined by Eqs. (10) and (11). σ_0^* in Eq. (12) stands for the initial total normal stress on the tested specimen, before applying the cyclic loading. Since the undrained condition is imposed only during the application of cyclic stresses, we have $\sigma_0^* = \sigma'_0$ for laboratory testing.

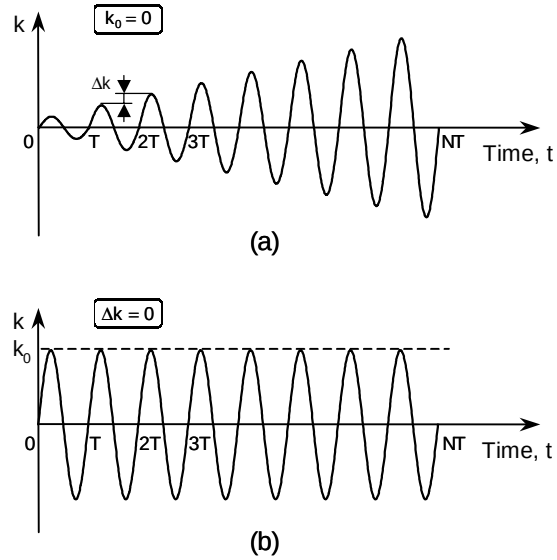

Fig. 5 (*a*) Increasing amplitude and (*b*) constant amplitude excitations used in undrained cyclic ring shear tests

2.5 Comparison of results from undrained monotonic and cyclic ring shear tests

Figure 6 depicts the displacement series data from undrained cyclic ring shear tests showing also, on each diagram, the results from undrained monotonic shearing corresponding to the same initial stress conditions. Experiments A1, A2, and B2 represent undrained cyclic ring shear tests under uniform loading (i.e., $\Delta k = 0$ in Eq. (9)) with shear stress amplitudes greater than the peak strength from undrained monotonic testing. Tests A1 and B2 correspond to cyclic loading conditions with no reversibility in driving shear stress (i.e., $\tau_d > 0$) during the experiment, whereas a greater loading amplitude was selected for test A2 in order to reach negative values of τ_d within every cycle of undrained loading. Experiment B1 addresses an undrained cyclic ring shear test with increasing amplitude of loading (i.e., $k_0 = 0$ in Eq. (9)) and no shear stress reversal.

A quick examination of the experimental results from tests A1, B1, and B2, illustrated in Fig. 6, reveals that the upper boundary of the unloading–reloading loops from the cyclic ring shear tests, follows very closely the shear resistance *vs.* shear displacement relationship from the undrained monotonic ring shear tests. The sand demonstrated a similar response also for the cyclic ring shear test A2, prior to the first unloading; thereafter, a slight decrease in the available cyclic shear strength may be noted compared with the monotonic shear response. Hence, it appears that the reversibility in driving shear stresses on the failure plane is responsible for a higher excess pore pressure generation, in spite of a positive cyclic shear resistance measured during the entire experiment. However, as a general overview, this laboratory study demonstrated that, for the tested sand, the shear resistance–displacement curve provided by the undrained monotonic ring shear test may be regarded as a reasonable estimate of the available shear strength under various cyclic loading conditions. This aspect is clearly emphasized by the experimental results presented in Fig. 6.

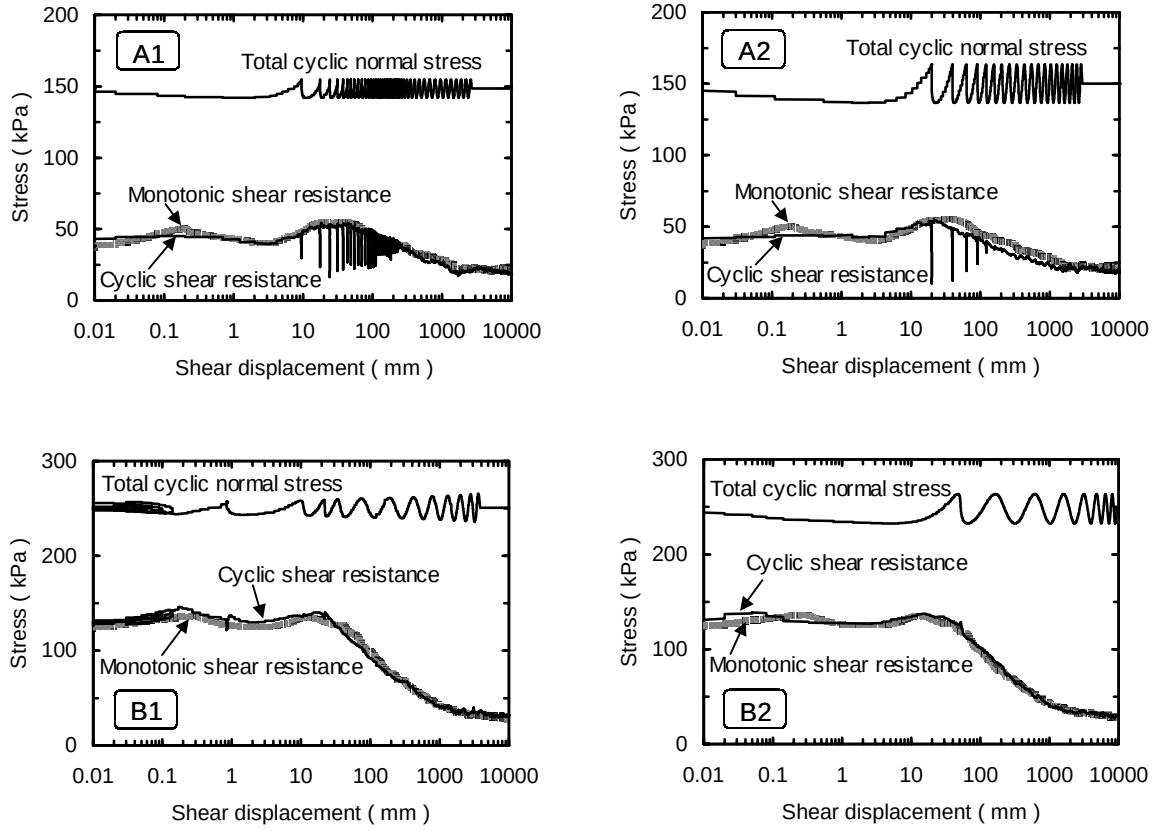

Fig. 6 Shear resistance from undrained monotonic and cyclic ring shear tests

3. Formulation

Assuming the sliding mass in Fig. 7 as a rigid body in translation on the sliding surface, driven by a horizontal seismic force, the Newton's second law of motion applied on the direction parallel to the slip surface yields

$$\frac{W}{g}\ddot{s} = W\sin\beta + kW\cos\beta - R \qquad (14)$$

where $\ddot{s}$ represents the acceleration of the sliding mass relative to the base, g is the gravitational acceleration, and R stands for the resistant force developed by the soil on the sliding surface. The latter may be written as

$$R = \tau_r\, b\, \sec\beta \qquad (15)$$

with τ_r defining the available soil shear strength.

Equation (14) leads to the final expression of the relative acceleration

$$\ddot{s} = (a - k_y\, g)\, \cos\beta \qquad (16)$$

in which a denotes the earthquake acceleration (a=kg), whereas k_y stands for the yield coefficient of the potential sliding mass given by Eq. (17):

$$k_y = \left(\frac{\tau_r}{\tau_0} - 1\right)\tan\beta \qquad (17)$$

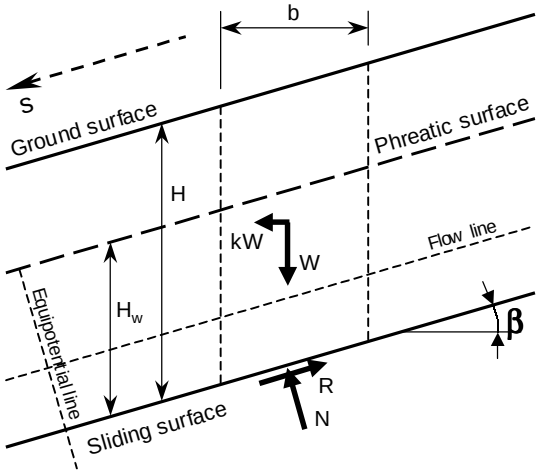

Fig. 7 Forces involved in the equation of motion

In a conventional Newmark procedure, k_y defines the coefficient of a pseudo–static seismic force necessary to cause the limit equilibrium of the potential sliding mass. Therefore, in the case of a dry cohesionless soil on the sliding surface, the expression of k_y is given solely by the soil effective friction angle, ϕ', and slope angle (e.g., Seed and Goodman, 1964; Goodman and Seed, 1966; Chugh, 1995), being thus constant in situations involving a perfectly plastic shear response after failure. Undrained conditions on the slip surface, however, imply that under seismic conditions, τ_r relates to the magnitude of shear displacement, as demonstrated by the laboratory study introduced in the previous section. Consequently, the yield capacity of the sliding mass will be correlated with the amount of earthquake–induced relative slope displacement at a certain instant during the seismic excitation. In order to include this aspect in an undrained dynamic analysis, the Newmark based approach proposed in this study utilizes the experimental data from undrained monotonic shearing to estimate the available undrained dynamic strength during earthquake. This assumption seems reasonable for the considered sand, since variations in total normal stress on the slip surface during earthquake appear to have no influence on the available undrained cyclic shear strength (see Fig. 6). As illustrated in Fig. 8*a*, by employing in the computational process the shear resistance–displacement curve from the undrained monotonic ring shear test, it is possible to estimate the amount of shear strength that can be developed by the soil on the sliding surface in undrained conditions, $\tau_r(t)$, given the value of earthquake–induced slope displacement, $s(t)$, at a certain instant during earthquake. In this circumstances, k_y in Eq. (17), may be interpreted as the coefficient of the pseudo–static seismic force corresponding to the equilibrium of the sliding mass at a certain magnitude of displacement.

The example of undrained monotonic shear response shown in Fig. 8*a*, corresponds to a saturated sandy soil with an ultimate steady state strength after failure (*USS*) below the static driving shear stress, τ_0. For materials on the slip surface exhibiting this type of undrained shear behavior, a critical moment during the seismic slope performance corresponds to the instant when the amount of earthquake–induced displacement reaches a critical level equal to s_0 in Fig. 8*a*. It is seen in Fig. 8*a* that displacements greater than s_0 involve available shear strengths below τ_0. Hence, a displacement at the end of seismic excitation exceeding the critical level, s_0, may result in a catastrophic slope failure, since there is a high probability that the sliding mass will continue to move even after the earthquake loading has ceased, assuming no significant changes in the static driving shear stress on the slip surface. This is more clearly illustrated in Fig. 8*b* addressing the yield coefficient in relation to displacement of the sliding mass, for the shear strength characteristics on the slip surface depicted in Fig. 8*a*. As shown in Fig. 8*b*, slope displacements beyond s_0 are associated with negative yield coefficients, suggesting that a pseudo–static seismic force acting towards the slope is necessary to keep the sliding mass in equilibrium.

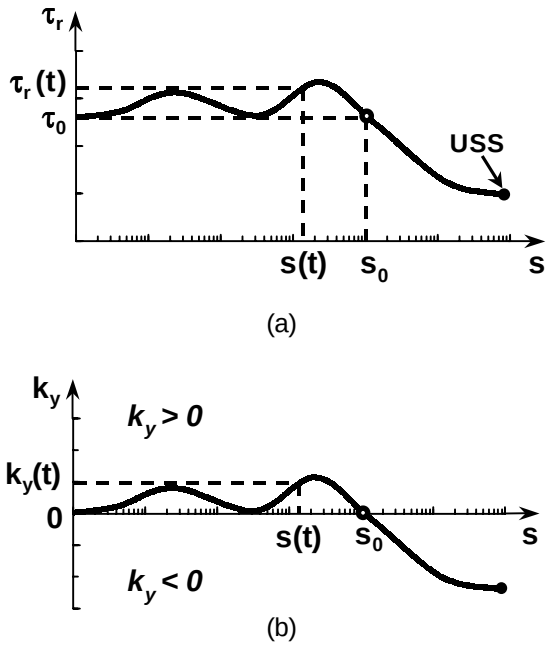

Fig. 8 (*a*) Example of undrained monotonic shear response and (*b*) the corresponding yield coefficient in relation to slope displacement

Equation (16) requires a step–by–step numerical integration to calculate the dynamic displacements. However, the presence of k_y depending on the unknown value of displacement, s, renders to Eq. (16) a nonlinear character. Therefore, an iterative computational procedure is necessary to obtain the solution.

4. Sample problem

The methodology introduced in the previous section has been used to investigate the seismic response of slopes A and B listed in Table 1, considering two input accelerograms plotted in Fig. 9. These seismic records, have been obtained during El Salvador earthquake, Magnitude M=7.6, on January 13, 2001, and Hyogoken–Nambu earthquake, Magnitude M=7.2, on January 17, 1995, respectively. In order to investigate the influence of input signal on the slope performance, both accelerograms were scaled to a coefficient of maximum earthquake acceleration, k_m, of 0.25 as shown in Fig. 9.

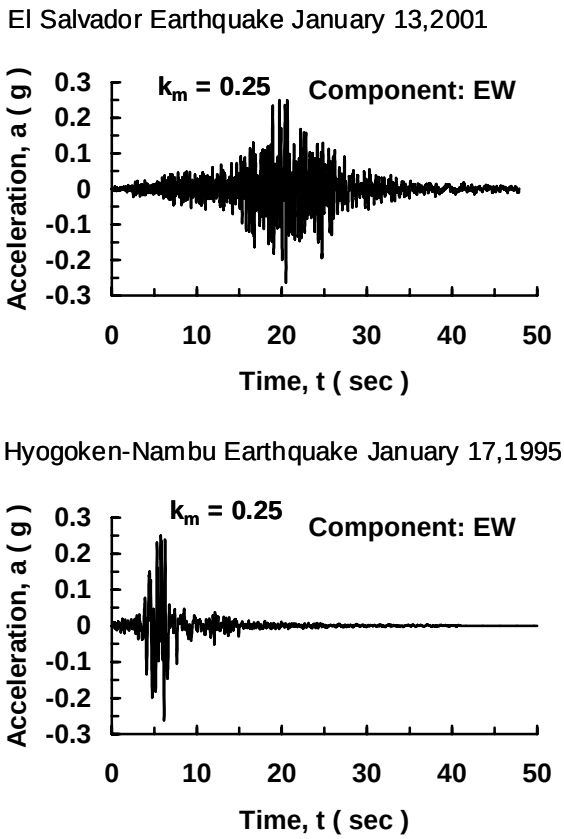

Fig. 9 Input earthquakes for sample problem

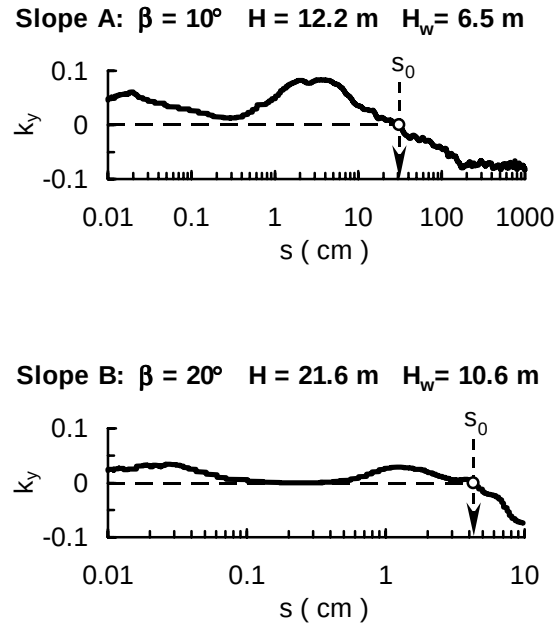

Fig. 10 Yield coefficient in relation to displacement for the analyzed slopes

Figure 10 depicts the yield coefficient in relation to the slope displacement based on the experimental curves shown in Fig. 3*b*, showing also, the critical displacement, s_0, necessary to cause a catastrophic failure of slopes A and B from Table 1.

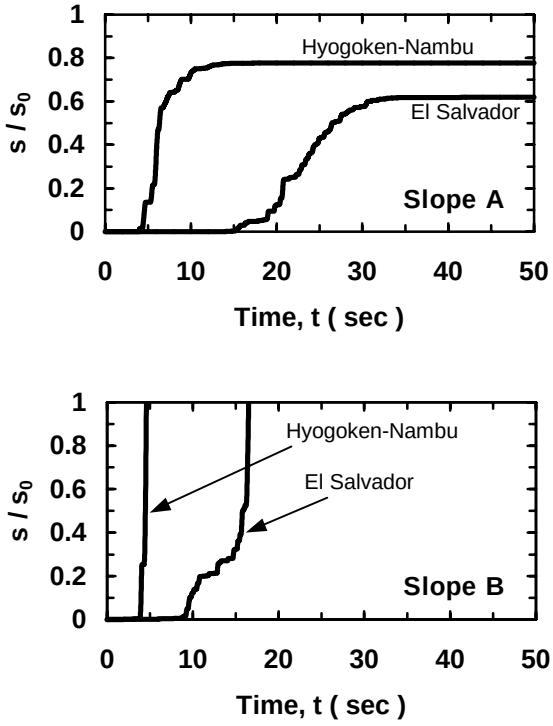

Fig. 11 Slope displacements from El Salvador and Hyogoken–Nambu earthquakes scaled to 0.25g

Examination of earthquake–induced undrained displacements of slope A in Fig. 11 reveals that the input signal affects the seismic slope response. As shown in Fig. 11, for k_m=0.25, the displacement of slope A at the end of El Salvador earthquake is about $0.6s_0$, whereas Hyogoken–Nambu earthquake resulted in a permanent displacement of $0.8s_0$. However, slope A performed well under the given seismic excitations, remaining stable after the earthquake. This aspect is more clearly illustrated in Fig. 12 showing the time history of driving shear stress, τ_d, and available shear strength, τ_r, on the sliding surface for El Salvador earthquake. It may be noticed in Fig. 11 that concerning slope A, τ_r just after the earthquake was slightly greater than τ_d, suggesting that no additional movement will take place under static conditions. Conversely, slope B demonstrated a sharp increase in displacements under both seismic excitations, reaching the critical stage before the peak of the strong ground motion (see Fig. 11). It is easy to imagine the damage potential of such a catastrophic slope failure, due to the high mobility of sliding mass, by examining the results of the analysis corresponding to slope B in Fig. 12. Apparently, the sliding mass reached a relative displacement of 10 m in less than 5 seconds after the critical displacement, s_0, has been reached, assuming no changes in topography. This result demonstrates the crucial role played by the softening of the material on the sliding surface upon the accelerated motion

of the sliding mass after the onset of a catastrophic slope failure.

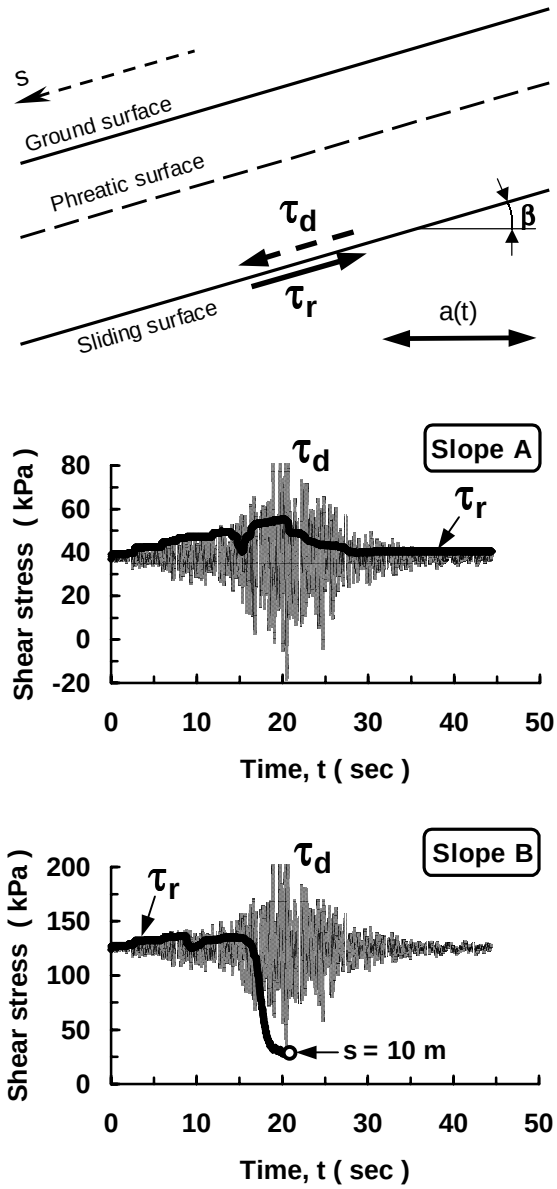

Fig. 12 Time history of driving shear stress, τ_d, and available shear strength, τ_r, on the slip surface for El Salvador earthquake scaled to 0.25g

5. Conclusions

The undrained shear behavior of a saturated clean sand under static and dynamic conditions has been investigated through a laboratory study based on monotonic and cyclic ring shear tests, with initial shear stresses greater than ultimate steady state strength. Examination of experimental results revealed that, for the tested sand, the shear resistance *vs.* shear displacement relationship from undrained monotonic ring shear tests may be considered a reasonable approximation of the available dynamic shear strength developed under cyclic loading conditions. This outcome of the laboratory study provided the experimental framework for a modified Newmark sliding block method to estimate the earthquake–induced undrained displacements of an infinite slope. The material assumed on the sliding surface was the saturated sand considered in the experimental study. Sample calculations demonstrated the effectiveness of a seismic analysis based on slope performance, capable to encompass the sensitivity of computed displacements to reductions in yield acceleration; resulting thus in a more reliable assessment of post-earthquake slope stability, when comparing with a traditional limit equilibrium approach, where the seismic loads are treated in a pseudo-static fashion. The proposed procedure may be used to predict whether a catastrophic landslide will initiate or not under given seismic conditions.

References

Ambraseys, N.N., and Menu, J.M. (1988): Earthquake–induced ground displacements, Journal of Earthquake Engineering and Structural Dynamics, Vol. 16, pp. 985–1006.

Cai, Z., and Bathrust, R.J. (1995): Deterministic sliding block methods for estimating seismic displacements of earth structures, Journal of Soil Dynamics and Earthquake Engineering, Vol. 15, pp. 255–268.

Chugh, A.K. (1995): Dynamic displacement analysis of embankment dams, Géotechnique, Vol. 45, No. 2, pp. 295–299.

Franklin, A.G., and Chang, F.K. (1977): Permanent displacement of earth embankments by Newmark sliding block analysis, Misc. Paper S-71-17, Soil and Pavements Lab., US Army Eng. Waterways Expt. Stn., Vicksburg, Miss.

Goodman, R.E., and Seed, H.B. (1966): Earthquake–induced displacements in sand embankments, Journal of the Soil Mechanics and Foundations Division, ASCE, Vol. 92, No. 2, pp. 125–146.

Ishihara, K. (1993): Liquefaction and flow failure during earthquakes, The 33rd Rankine Lecture, Geotechnique, Vol. 43, No. 3, pp. 351-415

Maksidi, F.I., and Seed, H.B. (1978): Simplified procedure for estimating earth dam and embankment earthquake–induced deformations, Journal of Geotechnical Engineering, ASCE, Vol. 104, GT 7, pp. 849–867.

Newmark, N.M. (1965): Effects of earthquakes on dams and embankments, Géotechnique, Vol. 15, No. 2, pp. 139–160.

Sarma, S.K. (1973): Stability analysis of embankments and slopes, Geotechnique, Vol. 23, No. 3, pp. 423–433.

Sassa, K. (1988): Motion of Landslides and Debris-Flows- Prediction of hazard area, Report for Grant-in-Aid for Scientific Research by Japanese Ministry on Education, Science and Culture, Project No. 61480062, pp. 15.

Sassa, K. (1996): Prediction of earthquake induced landslides, Special Lecture of 7th International Symposium on Landslides, *"Landslides"*, Rotterdam: Balkema, 1, 115-132.

Sassa, K. (1997): A new intelligent type of dynamic loading ring-shear apparatus, Landslide News, No. 10, pp. 33.

Sassa, K., Fukuoka, H. and Wang F.W. (1997a): A geotechnical simulation test on the Gamahara torrent debris flow with ring shear apparatus (in Japanese), Journal of the Earth, Vol. 19, No. 10, pp. 645-651.

Sassa, K. (2000): Mechanism of flows in granular soils, Invited paper, Proc. GeoEng2000, Melbourne. Technomic Publishing Company, Inc., Vol. 1, pp. 1671–1702.

Sassa, K. (2002): Mechanism of rapid and long traveling flow phenomena in granular soils, Proc. Int. Symp. on Landslide Risk Mitigation and Protection of Cultural and Natural Heritage, Vol. 1, pp. 11-29.

Sassa, K., Wang, G., and Fukuoka, H. (2002a): Performing undrained shear tests on saturated sands in a new intelligent type of ring shear apparatus, Geotechnical Testing Journal (*in press*).

Seed, H.B, and Goodman, R.E. (1964): Earthquake stability of slopes of cohesionless soils, Journal of Soil Mechanics and Foundations Division, ASCE, Vol 90, No. 6, pp. 43–73.

Wang, F.W. (1998): An experimental study on grain crushing and excess pore pressure generation during-shearing of sandy soils- A key factor for rapid landslide motion, Ph.D. Thesis, Kyoto University.

Wang, F.W., Sassa, K. and Fukuoka, H. (2000): Geotechnical simulation test for the Nikawa landslide induced by January 17, 1995 Hyogoken-Nambu earthquake, Soils and Foundations, Vol. 40, No. 1, pp. 35-46.

Wang, G., and Sassa, K. (2002): Post–failure mobility of saturated sands in undrained load–controlled ring shear tests, Canadian Geotechnical Journal, Vol. 39**,** pp. 821–837.

Yoshimine, M., Robertson, P.K., and Wride, C.E. (1999): Undrained shear strength of clean sands to trigger flow liquefaction, Canadian Geotechnical Journal, Vol. 36, pp. 891–906.